Radio Science, Volume 16, Number 5, pages 671–689, September–October 1981

Structures of atmospheric precipitation systems: A global survey

Robert A. Houze, Jr.

Department of Atmospheric Sciences, University of Washington, Seattle, Washington 98195

(Received May 26, 1980; accepted December 8, 1980.)

A survey of atmospheric precipitation systems, ranging from mid-latitude cyclones and thunderstorms to tropical cloud clusters, hurricanes, and monsoons, shows that all these systems are well described in terms of the rather traditional concepts of stratiform and convective precipitation. In stratiform precipitation, ice particles grow as they drift downward from high levels and pass through a well-defined melting layer. In convective precipitation, particles begin growing at low levels and are carried upward by strong updrafts and fall out in intense vertically oriented showers. Modern observations show that all the major types of precipitation observed over the globe can be and often are combinations of these two basic types of precipitation. Extratropical cyclonic precipitation is basically stratiform. However, it is typically intensified in regions called rainbands. Some rainbands are highly convective features which move through the basic stratiform precipitation. In other rainbands, shallow convective cells occur aloft and help to enhance the basic stratiform precipitation. Mid-latitude thunderstorms and tropical precipitation systems are basically convective. However, stratiform precipitation can develop in the middle to late stages of development. This type of stratiform precipitation, which can become quite extensive in both tropical and mid-latitude systems, apparently arises as groups or successions of active convective cells leave ice particles aloft to settle downward gradually after the cells' updrafts die out.

1. INTRODUCTION

For many years, meteorologists have considered precipitation to be of two basic types, stratiform and convective. *Houghton* [1968] clearly distinguished these two basic precipitation mechanisms in terms of the times available for the growth of precipitation particles and the magnitudes of the vertical air motions in the precipitating clouds.

In stratiform precipitation (Figure 1), the vertical air motions maintaining the cloud are sufficiently weak that, according to Houghton, '. . . precipitation particles fall with respect to the ground almost from their initiation and the most favorable region of initiation [to allow maximum time for subsequent growth] is at or near the top of the cloud system.' The particles forming at upper levels may drift downward slowly as they grow, especially at first, but this is not a problem since the stratiform system is long lived. The particles tend to form aggregates as they move downward, particularly as they approach to within ~1 km of the melting level [*Hobbs*, 1974, p. 641]. The melting layer is a very prominent feature appearing as a 'bright band' in radar reflectivity patterns and as a layer of strong gradient of fallspeed in Doppler radar displays.

Convective precipitation (Figure 2) occurs when vertical air motions are locally strong, e.g., when instability of the thermodynamic stratification of the atmosphere is released in the form of cumulus or cumulonimbus clouds. As pointed out by Houghton, the time it takes such clouds to develop precipitation is so short that precipitation particles need to be initiated and start growing near cloud base at the time the cloud forms (time t_0 in Figure 2). It is possible for the growth to begin at that time, since updrafts are strong enough to carry the growing particles upward until they become heavy enough to overcome the updraft and begin to fall relative to the earth (see the particle trajectory in Figure 2). Houghton hypothesized that the primary growth mechanism for these particles is accretion of cloud liquid water.

Radar returns from precipitation associated with active convection form well-defined vertical cores of maximum reflectivity, which contrasts markedly with the horizontal orientation of the radar bright band seen at the melting level in stratiform precipitation (compare the reflectivity patterns in Figures 1 and 2).

In the dissipating stages of precipitating convec-

Paper number 80S1743.
0048-6604/81/0910-1743$01.00

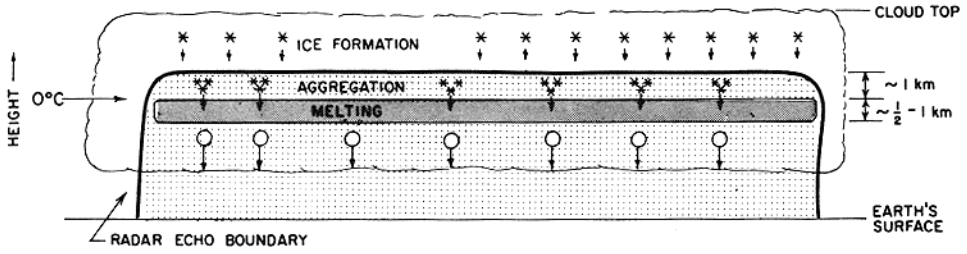

Fig. 1. Schematic of the stratiform precipitation process. Solid lines are contours of radar reflectivity, with the dark shading in the melting layer indicating the maximum reflectivity.

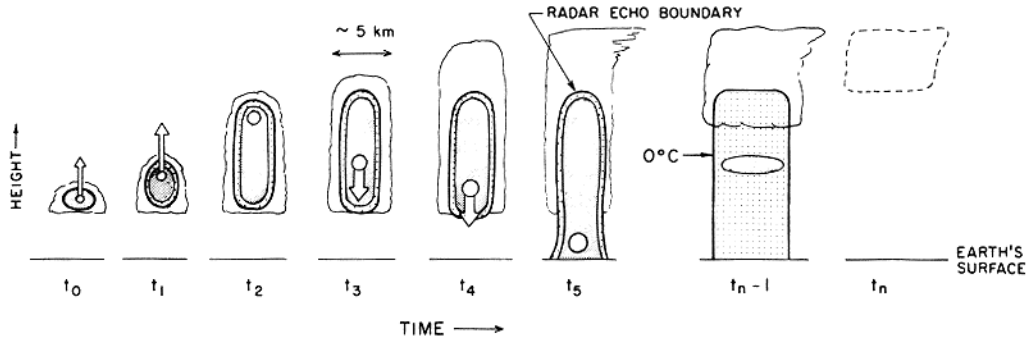

Fig. 2. Schematic of the convective precipitation process. Cloud is shown at a succession of times t_0, t_1, $\cdots$, t_n. Growing precipitation particle is carried upward by strong updrafts until t_2, then falls relative to the ground reaching the surface at t_5. After t_5, the cloud may die or continue for a considerable time in a steady state before dissipation sets in at t_{n-1} and t_n. The dashed boundary indicates an evaporating cloud. Solid lines are contours of radar reflectivity with the dark shading indicating the maximum return.

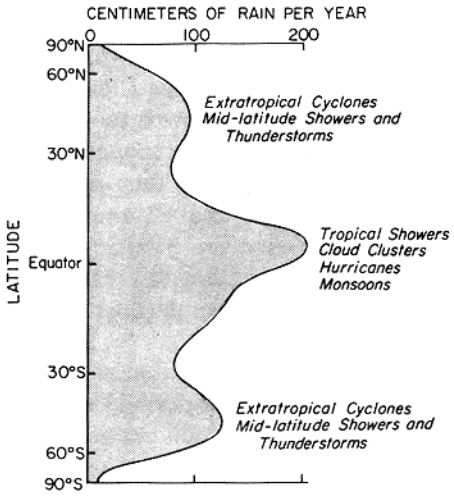

Fig. 3. Globally averaged annual precipitation. Types of weather systems associated with peaks are indicated (adapted from *Sellers* [1965]).

tive clouds (after time t_5 in Figure 2), strong upward motions cease and no longer carry precipitation particles upward or suspend them aloft. The fallout of the particles left aloft by the dying updrafts can take on a stratiform character, including a bright band (as noted by *Battan* [1973, p. 201]).

In this paper the traditional concepts of convective and stratiform precipitation mechanisms are examined in light of studies of actual storm structures. Many such studies, beginning with the Thunderstorm Project [*Byers and Braham,* 1949], have now been conducted, and during the 1970's, field studies involving aircraft and radar observations of precipitation systems reached high levels of sophistication. We shall consider how well the traditional stratiform and convective idealizations describe precipitation as it is actually seen to occur.

The types of precipitation systems that occur over the globe may be summarized by the climatological distribution of annual rain in Figure 3. As indicated, the maxima of precipitation in mid-latitudes are

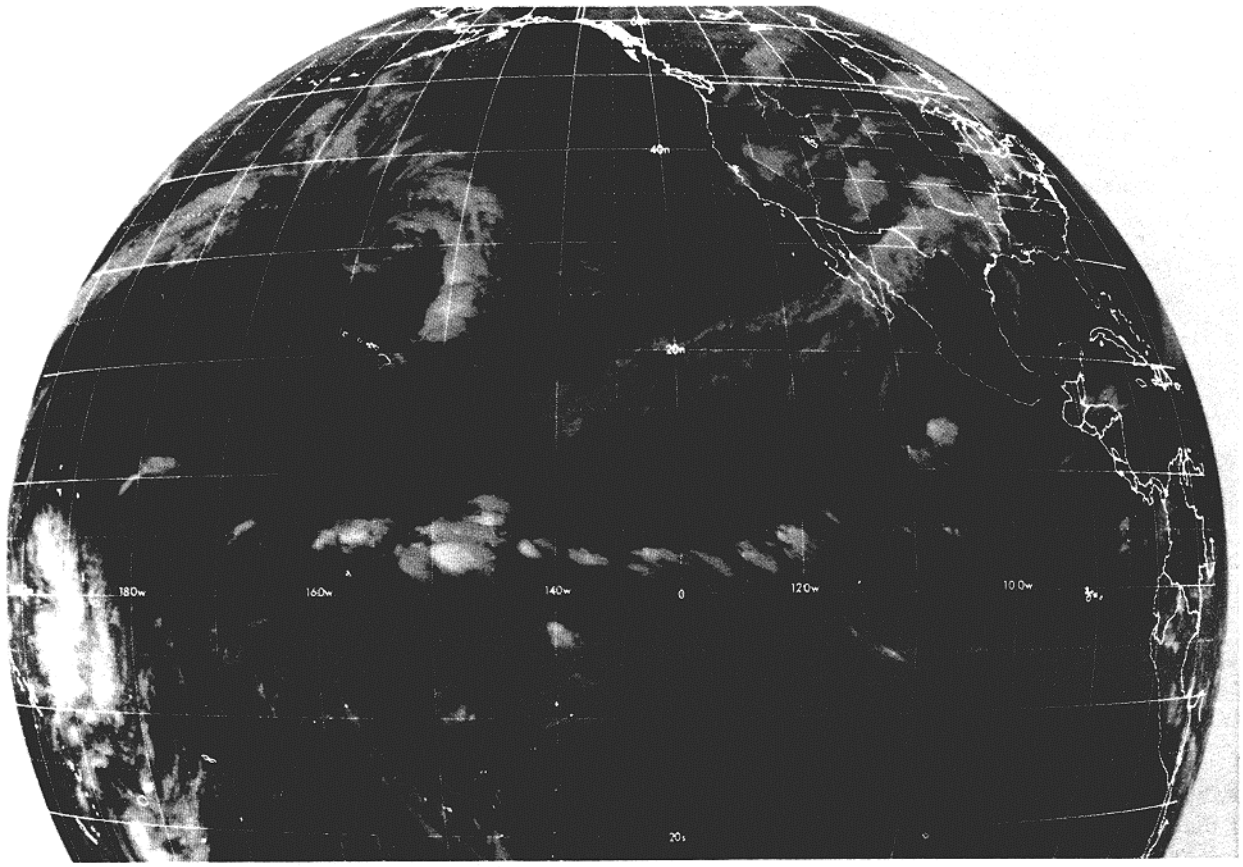

Fig. 4. Global infrared satellite photograph. Brightness is inversely related to temperature, so the tops of the highest clouds appear brightest (courtesy of National Oceanic and Atmospheric Administration).

associated with extratropical cyclones and mid-latitude showers and thunderstorms. Examples of extratropical cyclones are the large systems of curved cloud bands associated with storm centers over the central North and South Pacific oceans and over the western and south-central United States in Figure 4. The maximum of rainfall in the tropics indicated in Figure 3 is associated primarily with 'cloud clusters,' which are the patches of clouds concentrated in the zone of trade wind convergence that encircles the globe just north of the equator. In Figure 4 a chain of cloud clusters extends across the equatorial Pacific, with a particularly active area between 160°E and the international date line. Isolated rain showers, hurricanes, and monsoon rains also contribute to tropical precipitation. In Figure 4 a hurricane can be seen at 21°S,170°E (south of Fiji and east of New Caledonia).

In the following sections a global survey will be made in which examples of the structures of the various types of precipitation systems observed around the world will be examined, with particular emphasis on the extent to which they exhibit the characteristics of convective or stratiform precipitation processes.

2. EXTRATROPICAL CYCLONES

2.1 *Occurrence of rainbands*

The concept of the stratiform precipitation mechanism is most commonly used in describing the precipitation in extratropical cyclones. These storms, which are the familiar systems followed on daily weather maps, are characterized by fronts curving outward for thousands of kilometers from the storms' centers. Upward air motions are associated with the fronts, and clouds and precipitation forming in response to the lifting coincide in broad

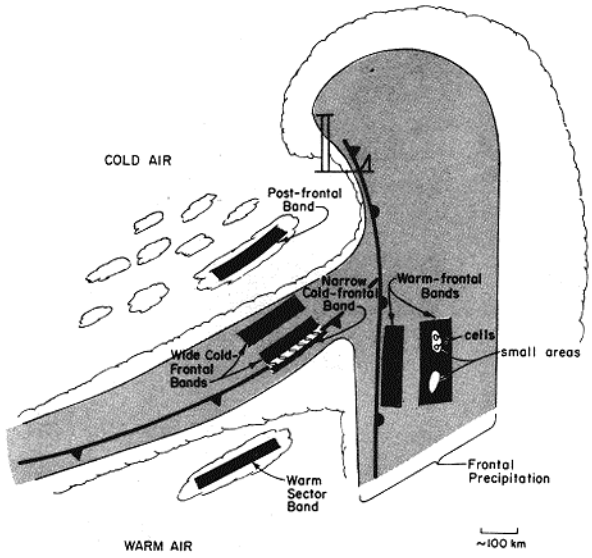

Fig. 5. Schematic of typical features of the cloud (scalloped boundary) and precipitation pattern of an extratropical cyclone. Low pressure center is indicated by L. Fronts are indicated by standard symbols.

outline with the patterns of the fronts (Figure 5). If the frontal air motions dominated the cloud and precipitation formation processes, then the precipitation region would be without further detail of horizontal structure.

Normally, however, considerable substructure is found within the basic frontal precipitation patterns. The major subfeatures are areas of more intense precipitation called rainbands [*Harrold and Austin,* 1974; *Browning,* 1974; *Houze et al.,* 1976*a*; *Hobbs,* 1978; *Matejka et al.,* 1980].

The typical horizontal scales and distribution of the main types of rainbands that occur in an extratropical cyclone are depicted schematically in Figure 5. The 'warm sector' and 'post frontal' rainbands occur outside the frontal precipitation area and can be considered lines of showers and thunderstorms like those considered in section 3. In the present section, only the rainbands within the frontal precipitation region will be considered. The 'warm frontal' and 'wide cold frontal' rainbands are structurally similar except for their orientations, parallel to the warm and cold fronts of the cyclone, respectively. The controlling factor in their orientations may be the vertical wind shear [*Kreitzberg and Brown,* 1970], which between the 3-km and 6-km levels is often parallel to fronts if they are present. The 'surge' rainbands noted by *Matejka et al.* [1980] (not depicted in Figure 5) occur closer to the cyclone center than the bands indicated in Figure 5 and exhibit a slightly different orientation from that of the warm frontal and wide cold frontal rainbands but otherwise appear to be essentially the same type of feature. The warm frontal, wide cold frontal, and surge rainbands contain a hierarchy of weak smaller structures [*Harrold and Austin,* 1974] referred to as 'small areas' and 'cells' in Figure 5.

The 'narrow cold frontal' rainband (whose appearance on radar was first described by *Kessler and Wexler* [1960]) is distinctly different from the other rainbands. It is very narrow (~1–5 km across) but may extend lengthwise for over a thousand kilometers [*Browning and Harrold,* 1970]. It contains heavy precipitation, moves with the leading edge of the cold front, and consists of a series of small elements oriented at a slight angle to the front [*Hobbs and Biswas,* 1979; *James and Browning,* 1979]. The narrow cold frontal rainband moves independently of the other rainbands (the latter apparently being steered by winds aloft) and, as depicted schematically in Figure 5, occasionally crosses over one or more of them [*Houze et al.,* 1976*a*; *Hobbs et al.,* 1980].

2.2 *Large-scale cyclonic precipitation structure*

To a large extent, understanding the precipitation processes in extratropical cyclones involves understanding how the rainbands operate. Before proceeding to an examination of the bands themselves, however, let us consider the larger-scale general frontal precipitation in which they are embedded. Figure 6 shows a time cross section of vertically pointing Doppler radar data obtained during the passage of a cyclonic storm similar to the one shown schematically in Figure 5. Although four rainbands were embedded in the precipitation, a basic stratiform structure, with a well-defined melting band evident in the vertical gradient of the precipitation fallspeed, existed continuously across the whole storm. The melting layer rose slightly as the warm frontal portion of the storm passed, then lowered again as the cold frontal region went by. As each rainband passed over the radar, an increase in mean fallspeed at lower levels was measured. Nonetheless, the basic vertical layering of the precipitation remained intact. These rainbands (warm frontal and

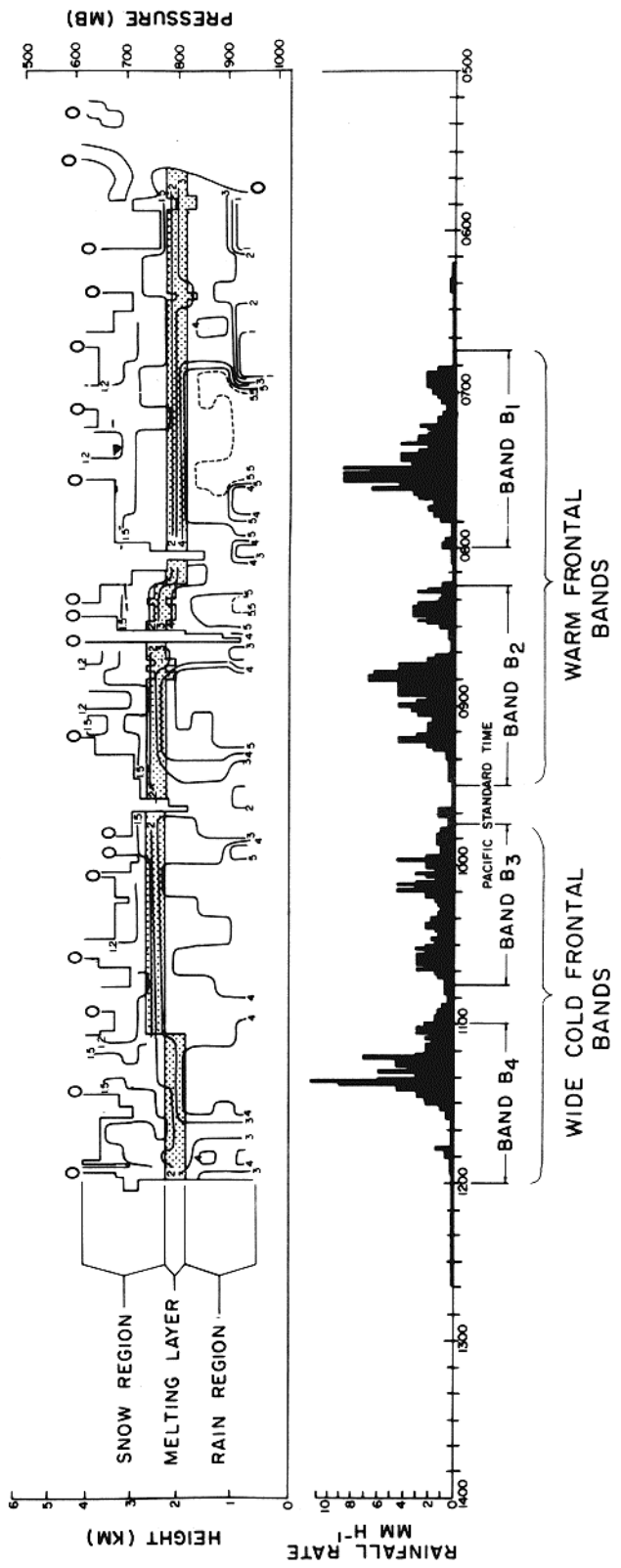

Fig. 6. Vertical cross section showing contours of 10 min average precipitation fall speeds (m s^{-1}) measured with Doppler radar and high-resolution rainfall trace (mm h^{-1}) obtained at the radar site. Melting layer, characterized by a large gradient of fall speed, is shaded for emphasis in the cross section. Contours labeled with zeroes outline the region of precipitation detected by the radar (adapted from *Houze et al.* [1976*b*]).

wide cold frontal) can be regarded, therefore, as region of intensification of the basic stratiform precipitation.

2.3 *Example of a stratiform rainband*

The way in which the basic stratiform precipitation becomes intensified can be seen in the cross section through a warm frontal rainband shown in Figure 7. Doppler radar and rawinsonde measurements of the airflow through this rainband allowed aspects of its water budget to be determined. Two factors were found to be important in the local intensification of the stratiform precipitation. Firstly, the general rate of upward air movement was enhanced at low levels. This lifting was producing cloud liquid water below the −4°C level at a rate sufficient to account for 65% of the surface rainfall. Formation of ice particles aloft, a necessary aspect of the stratiform precipitation process (Figure 1), was evidently occurring in convective 'generating' cells of the type normally associated with stratiform precipitation [*Battan,* 1973, pp. 195–197]. Direct aircraft sampling at the 3-, 4-, and 5-km levels indicated that the particles falling from the cells grew at first by a combination of deposition and slight riming, then, as they approached the melting level, by aggregation. As these large ice particles and the drops formed from their melting fell through

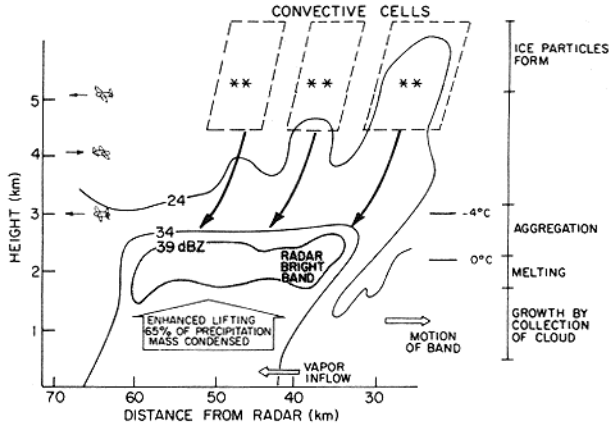

Fig. 7. Vertical cross section through a warm frontal rainband observed approaching the Washington coast on December 13, 1977. Radar echo contours are labeled in dBZ. The region of enhanced lifting was inferred from Doppler radar measurements. Arrows aloft indicate probable ice particle trajectories. Aircraft penetrations were made at the indicated flight levels (adapted from *Houze et al.* [1981]).

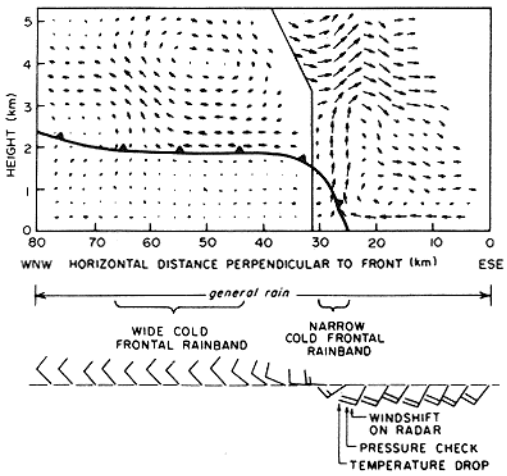

Fig. 8. Vertical cross section showing the airflow relative to a cold front as it was observed with Doppler radar. The arrows represent 5-min displacements. The heavy vertical seam separates airflows calculated from two different radar scans, 30 min apart, which have been joined to produce a composite picture. The cold front advancing from WNW to ESE is indicated by the standard symbol. The position of the windshift at the surface detected with radar is indicated at the bottom of the figure. Also shown are a wind record and other surface information from the radar site, positioned along the cross section using the speed of the front to convert time to distance (from *Matejka et al.* [1980]).

lower levels, they evidently accreted the cloud water condensing at low levels. Thus the lifting, which was responsible for the condensation at low levels, and the convective cells aloft cooperated to intensify the precipitation, with the increased lifting providing moisture for the particles initiated aloft to scavenge on their way to the surface.

2.4 *Narrow cold frontal rainbands*

The narrow cold frontal rainband is an essentially convective rather than stratiform feature. As can be seen from the Doppler radar detected airflow in Figure 8, it arises from convergence at the leading edge of the surface cold front and, as pointed out by *Browning and Harrold* [1970], may be forced rather than free convection. Whatever its origin, a narrow updraft (vertical velocity up to a few meters per second) penetrates up through the background stratiform cloud and precipitation. In another example (Figure 9), a narrow cold frontal rainband embedded within a wide cold frontal rainband was penetrated by a research aircraft. An updraft of 2–3 m s^{-1} was encountered between A

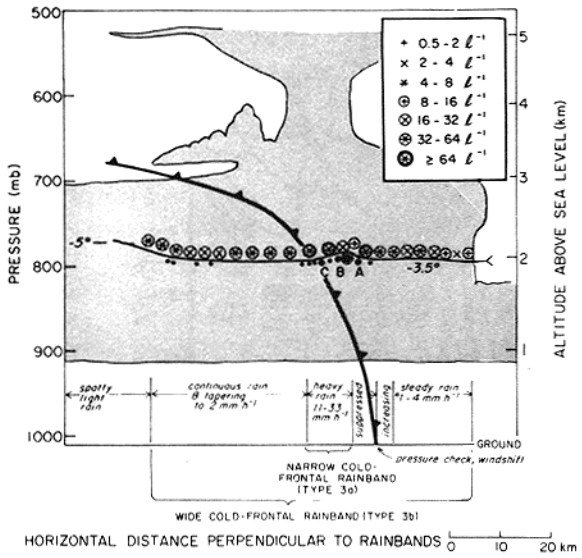

Fig. 9. Vertical cross section through a mesoscale cold frontal rainband penetrated by an instrumented aircraft, whose path is shown by the continuous arrowed line. Small, medium, and the circumscribed large dots on the flight path denote cloud liquid water contents from 0.10 to 0.20, 0.25 to 0.50, and ≥1.00 g m^{-3}, respectively. Symbols for ice particle concentrations are indicated by stars, as shown in the inset (from *Matejka et al.* [1980]).

and B. Immediately behind the updraft (B–C) was a downdraft of similar magnitude and width. The cloud and precipitation particles sampled in this and other narrow cold frontal rainbands (see *Matejka et al.* [1980] for other examples) are characteristic of young, vigorous convective cloud elements. The presence of considerable amounts of supercooled water (peak values of 0.45–1.40 g m^{-3}), apparently generated by the strongly ascending air motions, indicates the potential for the growth of precipitation particles by accretion of cloud liquid water, as postulated by *Houghton* [1968]. This potential was confirmed directly by airborne observations of graupel (that is, small hail) and other heavily rimed ice particles.

The structure of the narrow cold frontal rainband, with its strong updraft, high liquid water content and growth of precipitation particles by accretion of liquid water contrasts sharply with the stratiform cloud and precipitation in which it is embedded. For example, the wide cold frontal rainband, outside of the narrow cold frontal rainband contained only occasional patches of cloud liquid water of 0.1–0.2 g m^{-3} and ice particles sampled at flight level (≈0.5 km above the top of the melting layer) indicated that, in accordance with Figure 1, aggregation was the dominant precipitation mechanism rather than riming.

3. MID-LATITUDE THUNDERSTORMS

3.1 *The 'Thunderstorm Project' and air mass thunderstorms*

Interest in the origins and inner workings of thunderstorms extends back many centuries. For example, the ancient philosophers Anaxagorus and Aristotle once engaged in a controversy on the formation of hail in storm clouds [*Anthes et al.*, 1978, pp. 4–5]. Speculations on thunderstorms were aided by the introduction, about a century and a half ago, of observing stations for weather analysis and forecasting, but the routine observations obtained at these stations could not really resolve the storms' structures satisfactorily. The modern study of thunderstorms began with the use of instrumented aircraft and radars in the U.S. Government's Thunderstorm Project [*Byers and Braham*, 1949].

The Thunderstorm Project investigated the common summertime thunderstorms of Florida and Ohio. These 'air mass' storms form almost daily during summer over much of the United States, particularly in the southeastern part of the country. They occur in widespread convectively unstable air masses characterized by low-level warm humid air and little vertical wind shear. These storms are

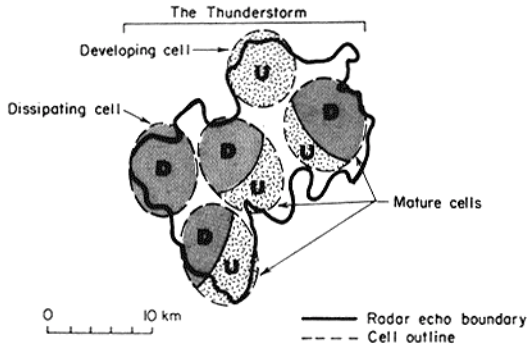

Fig. 10. Plan view of an ordinary air mass thunderstorm observed in Ohio during the Thunderstorm Project at 1420 EST on August 14, 1947. Developing cells contain updrafts (U), mature cells contain both updrafts and downdrafts (D), and dissipating cells contain only downdrafts (adapted from *Byers and Braham* [1949]).

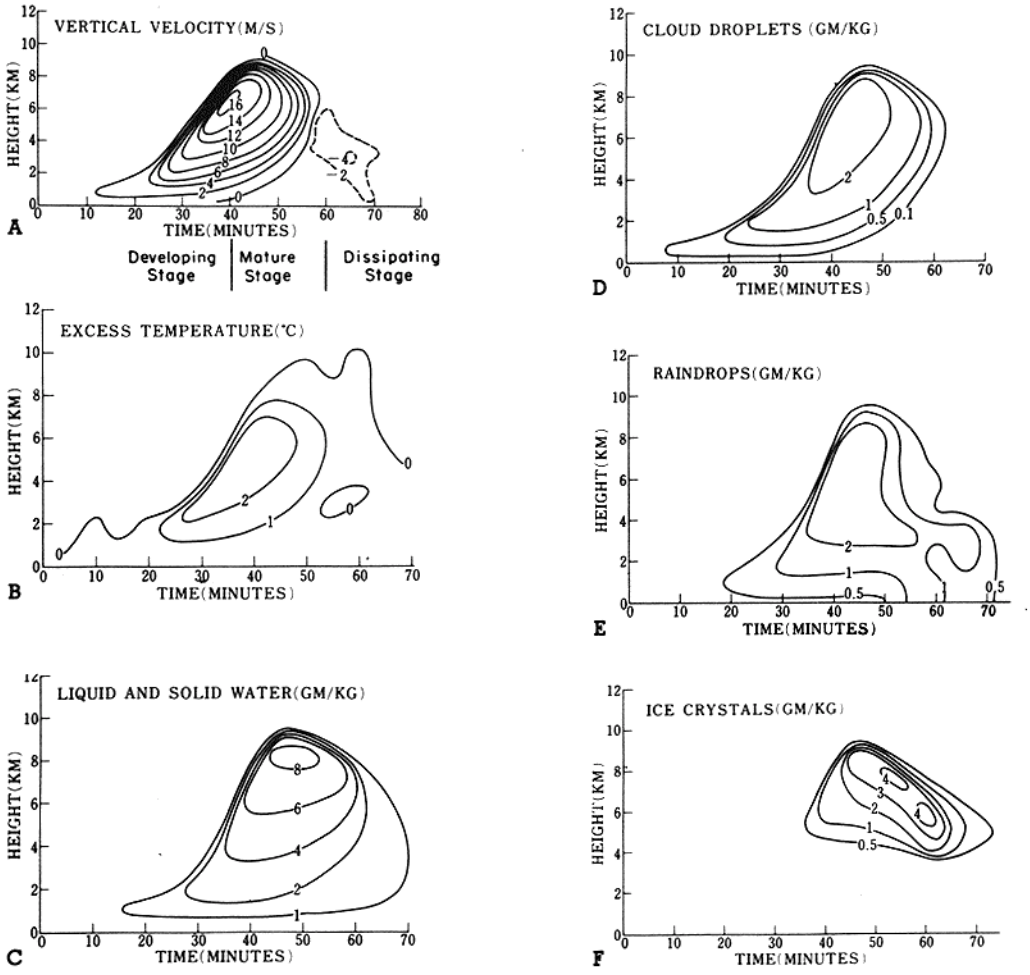

Fig. 11. Time height cross sections of (*a*) vertical velocity, (*b*) excess temperature, (*c*) liquid and solid water content, (*d*) content of cloud droplets, (*e*) content of raindrops, and (*f*) content of ice crystals for a thunderstorm cell simulated by a one-dimensional, time-dependent cloud model (from *Ogura and Takahasi* [1971]).

evidently triggered by transient disturbances within these air masses.

The internal structure of an individual air mass thunderstorm was found to be characterized by a more or less random pattern of 'cells,' which were the storm's basic convective units (Figure 10). It was deduced, moreover, that each cell within a thunderstorm progressed through a characteristic life cycle. In the Thunderstorm Project this cycle was synthesized from the various observations. Since then, the life cycle of a single cell within a thunderstorm has been simulated quantitatively in numerous cloud models. For example, *Ogura and Takahashi* [1971] used a simple model that computes the areal averages of in-cloud properties at a series of heights in a cylindrical cell. Their results illustrate in fairly realistic manner the three stages in the life cycle of a thunderstorm cell (Figure 11).

The developing stage (called the 'cumulus' stage by *Byers and Braham* [1949]) is characterized by a growing cloud pushing its way up toward its maximum height (Figure 11*d*). The interior of the cell at this stage is filled with buoyant air (Figure 11*b*) moving upward (Figure 11*a*). Precipitation particles begin developing early and near cloud base, as postulated by *Houghton* [1968] for convective clouds but do not yet reach the ground (Figure

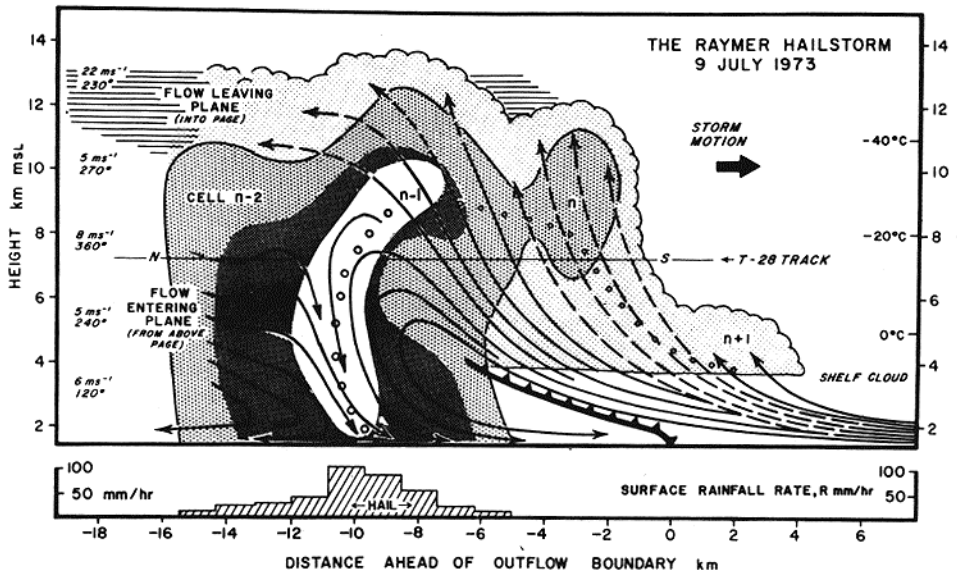

Fig. 12. Schematic model of an ordinary multicell hailstorm near Raymer, Colorado. It shows a vertical section along the storm's north to south (N-S) direction of travel, through a series of evolving cells. The solid lines are streamlines of flow relative to the moving system; they are shown broken on the left side of the figure to represent flow into and out of the plane and on the right side of the figure to represent flow remaining within a plane a few kilometers closer to the reader. The chain of open circles represents the trajectory of a hailstone during its growth from a small particle at cloud base. Lightly stippled shading represents the extent of cloud and the three darker grades of stippled shading represent radar reflectivities of 35, 45, and 50 dBZ. Winds (m s^{-1}, deg) on the left side are environmental winds relative to the storm (from *Browning et al.* [1976]).

11*e*). The tendency of the precipitation particles to fall is offset in this early stage by the strong updraft.

Eventually, the weight of the precipitation particles becomes considerable, and their drag on the air initiates a negatively buoyant downdraft in the lower portion of the cell. The appearance of this downdraft (at 40 min in Figure 11*a*) marks the beginning of the 'mature' stage of the cell, in which updraft and downdraft coexist. Losing their supporting upward motion, the precipitation particles begin reaching the ground (50 min in Figure 11*e*).

The disappearance of the updraft (after 60 min) defines the beginning of the 'dissipating' stage of the cell. During this stage, a weak downdraft persists until the remainder of the precipitation falls out as light rain.

3.2 *Severe thunderstorms*

The term 'severe' is used to describe thunderstorms bearing especially damaging hail and high winds. These storms differ from air mass thunderstorms in that they occur in environments of strong vertical wind shear. They are of two basic types, referred to as 'multicell' and 'supercell' storms.

The multicell severe storm is similar to the air mass thunderstorm investigated in the Thunderstorm Project, except that the cells form and move through the storm in a systematic and organized rather than random fashion. This process is illustrated by Figure 12, which can be thought of either as an instantaneous picture of a storm with cells in various stages of development or as a sequence of stages in the life of one cell as it moves, in a relative sense, through the storm. New cells (at $n + 1$ in Figure 12) form on or just ahead of the leading edge of the storm. At $n + 1$ and n, the cell is in a developing stage, similar to that of an air mass thunderstorm cell, with updraft air filling the cell and precipitation particles developing aloft but not yet falling to the ground. As hypothesized by *Houghton* [1968], precipitation particles begin near cloud base ($n + 1$) and grow by collection of supercooled cloud water. Above the 0°C level,

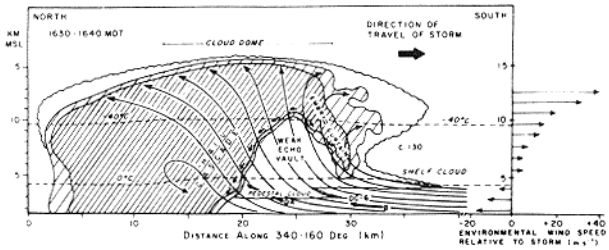

Fig. 13. Vertical section showing features of the visual cloud boundaries superimposed on the radar echo pattern of a supercell thunderstorm in northeastern Colorado. The section is oriented along the direction of travel of the storm, through the center of the main updraft. Two levels of radar reflectivity are represented by different densities of hatched shading. Areas of cloud devoid of detectable echo are shown stippled. The locations of four instrumented aircraft are indicated, viz., D-130, QA (Queen Air), DC-6 and B (Buffalo). Bold arrows denote wind vectors in the plane of the diagram as measured by two of the aircraft (scale is only half that of winds plotted on right side of diagram). Short thin arrows skirting the boundary of the vault represent a hailstone trajectory. The thin lines are streamlines of airflow relative to the storm drawn to be consistent with other observations. To the right of the diagram is a profile of the wind component along the storm's direction of travel, derived from a sounding 50 km south of the storm (from *Browning and Foote* [1976]).

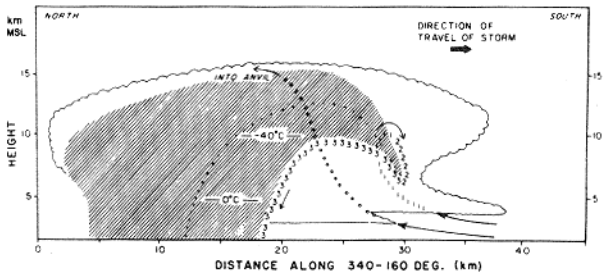

Fig. 14. Vertical section corresponding to Figure 13. The echo distribution and cloud boundaries are as before. Trajectories 1, 2, and 3, represent the three stages in the growth of large hailstones. The transition from stage 2 to 3 corresponds to the re-entry of a hailstone embryo into the main updraft prior to a final up-and-down trajectory during which the hailstone may grow large, especially if it grows close to the boundary of the vault as in the case of the indicated trajectory 3. Other less favored hailstones will grow a little farther from the edge of the vault and will follow the dotted trajectory. Cloud particles growing within the updraft core are carried rapidly up and out into the anvil along trajectory 0 before they can attain precipitation size (from *Browning and Foote* [1976]).

the collectors are primarily ice particles, whose growth, after their formative stages, is dominated by the accumulation of rime ice, which forms as cloud liquid water is accreted. Continuation of this riming builds up graupel particles and hailstones, which eventually become big enough to fall relative to the ground [*Dye et al.*, 1974].

At $n - 1$, the cell in Figure 12 has the characteristics of a mature thunderstorm cell: its maximum height has been attained, the updraft in its upper regions coexists with a strong downdraft at lower levels and heavy precipitation including hail, is reaching the ground. By $n - 2$, the cell has the characteristics of a dissipating cell: the updraft has disappeared, weak downdraft exists throughout the cell and precipitation, though still falling, is considerably weakened.

The organized arrangement of cells in the multicell severe storm is either superimposed on or together constitutes a circulation pattern on the scale of the thunderstorm itself. This circulation is evidently made possible by the ambient wind shear. It is characterized by general ingestion and upward flow of warm moist air entering the storm at low levels on its leading edge and exiting at upper levels from the rear. Dry mid-tropospheric air enters at the rear, is cooled as precipitation particles evaporate into it, and sinks in a broad downdraft, which occupies nearly the whole lower portion of the storm. As the downdraft air spreads out at the surface, it runs under the inflowing updraft air, helping force it upward to its level of free convection.

Whether the larger, storm-scale updraft-downdraft pair of the severe multicell thunderstorm constitutes a circulation pattern physically distinct from the individual cells or is simply an agglomeration of the air motions of the cells closely spaced in order of their successive stages of development is not clear. Whichever the case, the larger storm-scale circulation becomes more pronounced the greater the severity of the thunderstorm. Tornadoes and the largest hail are usually associated with 'supercell' thunderstorms, in which the individual cells lose their identity and the storm-scale circulation becomes particularly strong.

The supercell storm takes on the character of a single giant quasi-steady thunderstorm cell. In the example in Figures 13 and 14, the radar echo is one solid mass of high reflectivity in which cells are not evident. Except for the overhanging echo toward the front of the storm, the echo may be considered one huge shaft of convective precipitation. The massive updraft is qualitatively similar

to the storm-scale updraft in the leading portion of the multicell severe storm (Figure 12). The strength of the updraft is so great that cloud particles forming near the updraft base are carried to a great height before they grow to a size detectable by radar; hence the 'weak echo vault' appears in the updraft core. As in smaller convective cells, the growth of precipitation particles begins at cloud base. Various particle trajectories can ensue depending on where the particles are initiated. Those forming in the core of the updraft and following trajectory 0 in Figure 14, are carried aloft and into the storm's anvil cloud before becoming large enough to fall out. Particle 1, forming near the front edge of the updraft falls back into the updraft for a second cycle of growth by accretion of cloud liquid water before it is carried over to the rear of the storm, where the largest particles–often giant hailstones–fall at the front edge of the convective precipitation shaft (trajectory 3), while smaller ones are carried farther back into the precipitation shaft (dotted trajectory).

It should be noted that, although it is a useful idealization, the distinction between supercell and multicell thunderstorms is not really sharp. *Foote* [1977] points out 'that many important hailstorms do not fit either category very well, but rather have attributes of both classes.' *Browning and Atlas* [1965] described a multicell storm that evolved into a supercell, and *Lemon* [1976] described a supercell thunderstorm that propagated during part of its lifetime by successive incorporation of cells from a neighboring line of radar echoes, much as a multicell storm propagates.

In Figures 12–14 the supercell and multicell thunderstorms are viewed in two-dimensional vertical planes, which illustrate the essential features of their precipitation structure (our present objective). These storms, however, exhibit considerable three-dimensionality. For example, the formation of new cells on the leading edge of multicell storms generally occurs preferentially on one flank or the other (usually the right flank) of the thunderstorm, giving the storm a propagation velocity that deviates from the velocity of the mean tropospheric wind [*Newton and Fankhauser,* 1975], and the giant updraft and downdraft of the supercell are typically intertwined in a three-dimensional structure consistent with the wind in the environment of the storm [*Browning,* 1964; *Marwitz,* 1972]. An especially significant aspect of the supercell storm is the tendency of its large updraft to rotate cyclonically and spawn tornadoes [*Lemon et al.,* 1978; *Brown et al.,* 1978].

3.3 *Squall lines*

An interesting property of mid-latitude thunderstorms is their tendency to occur in lines, especially ahead of cold fronts (Figure 15). In the Thunderstorm Project, members of squall lines were found to be essentially similar to other thunderstorms. However, squall lines tend to occur in regions of significant vertical wind shear, and, consequently, individual members of lines tend to behave more as severe multicell or supercell storms than as air mass thunderstorms.

The precipitation structure of mid-latitude squall line thunderstorms is, therefore, much like those in Figures 12–14. Occasionally, however, a squall line will develop a wide region of lighter, more stratiform precipitation to the rear of its highly convective leading portion. This tendency can be seen in Figure 16, where the radar echo to the rear of the large updraft of the squall line thunderstorm had become horizontally uniform and was showing a bright band just below the melting level. Apparently, the leading portion of the storm can propagate into the region ahead in such a way that it leaves behind air loaded with precipitation which falls out in a stratiform manner typical of decaying convective elements (Figure 2).

The region of light precipitation to the rear of

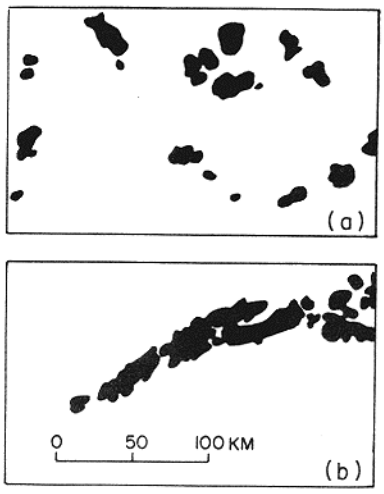

Fig. 15. Horizontal maps of radar echoes in cases with random (*a*) and squall-line (*b*) thunderstorms (from *Byers and Braham* [1949]).

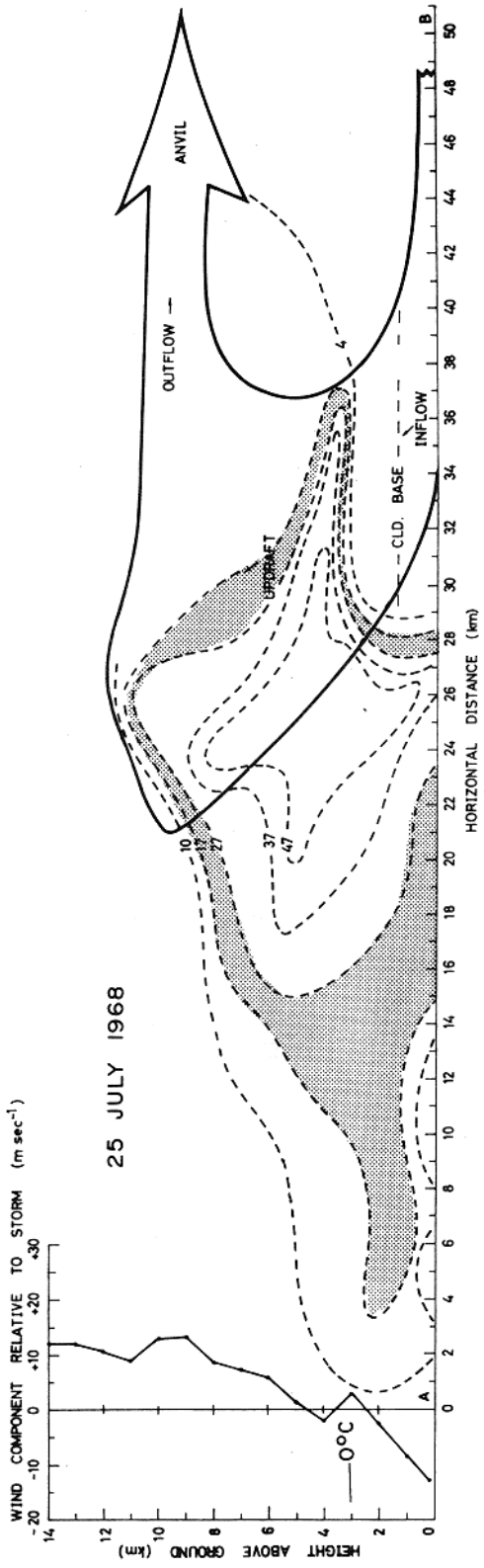

Fig. 16. Airflow of an Alberta squall line superimposed on its radar reflectivity pattern (dashed contours labeled in dBZ) in the plane of storm motion. Wind components relative to the storm (in the plane of storm motion) are shown on the left-hand side of the figure. Shading of the 17-27-dBZ region shows a bright band to the rear of the storm (from *Chisholm* [1973]).

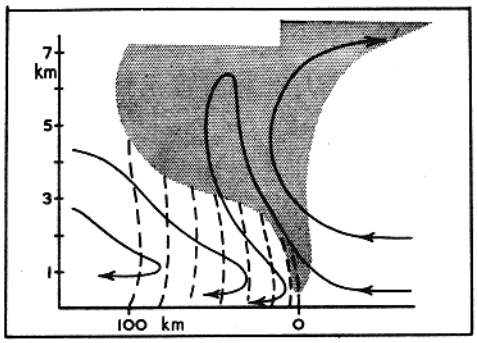

Fig. 17. Circulation relative to an Ohio squall line; stippled region is cloud, and dashed lines are precipitation (adapted from *Newton* [1950] and *Ludlam* [1963]).

the convective portion of squall line storms can be quite extensive. Squall lines studied by *Newton* [1950] and *Ogura and Liou* [1980] had trailing regions of lighter rain 100–150 km in width (Figures 17 and 18). The rain to the rear of the storms falls from a mid-tropospheric cloud base, below which is a wide downdraft apparently driven by cooling of the air by evaporation of the falling precipitation. Ogura and Liou's exceptionally well-documented case showed general uplift maintaining the trailing mid-to-upper tropospheric cloud from which the apparently stratiform trailing precipitation was falling.

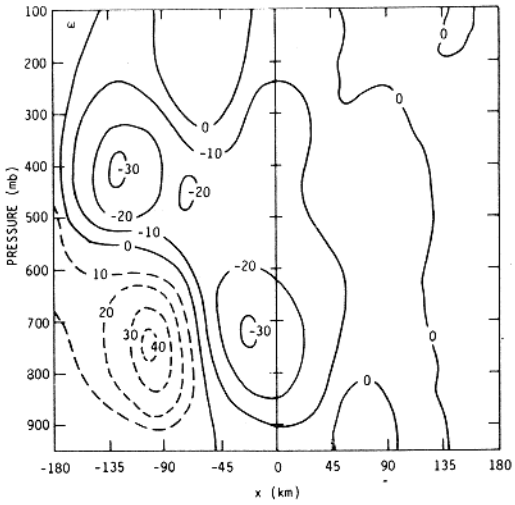

Fig. 18. Vertical air motion in a plane normal to an Oklahoma squall line. Units are 10^{-3} mbar s^{-1}. Negative values indicate upward motion. Positive values indicate downward motion; x represents distance ahead of the leading edge of the squall line (from *Ogura and Liou* [1980]).

4. TROPICAL PRECIPITATION

4.1 *Cloud clusters*

Precipitation in the tropics is almost wholly convective in origin; however, the rain falls in individual storms of a spectrum of sizes, ranging from isolated, small but numerous showers, a few square kilometers in area, to large cloud clusters, which contain rain areas covering up to $\approx 5 \times 10^4$ km^2 in area [*López,* 1976; *Houze and Cheng,* 1977]. The cloud clusters are the least numerous, but owing to their large size, they account for the bulk of the rainfall.

Two types of cloud clusters are recognized. Squall clusters are associated with tropical squall lines of the type first described by *Hamilton and Archbold* [1945] and later elaborated on by *Zipser* [1969] and others. They are notable in geosynchronous satellite imagery by their rapid propagation (≈ 15 m s^{-1}) and, according to *Payne and McGarry* [1977], by their 'explosive growth, high brightness and distinct and generally convex shaped leading edge.' Non-squall clusters do not form as dramatically or propagate as rapidly (typically only a few meters per second) as the squall clusters; however they are important, because they are so numerous. The squall clusters are relatively rare.

An example of the development of a squall cluster (Figure 19) shows the initial appearance at 1000 GMT on September 4, 1974, of a line of convective precipitation on radar with only a small amount

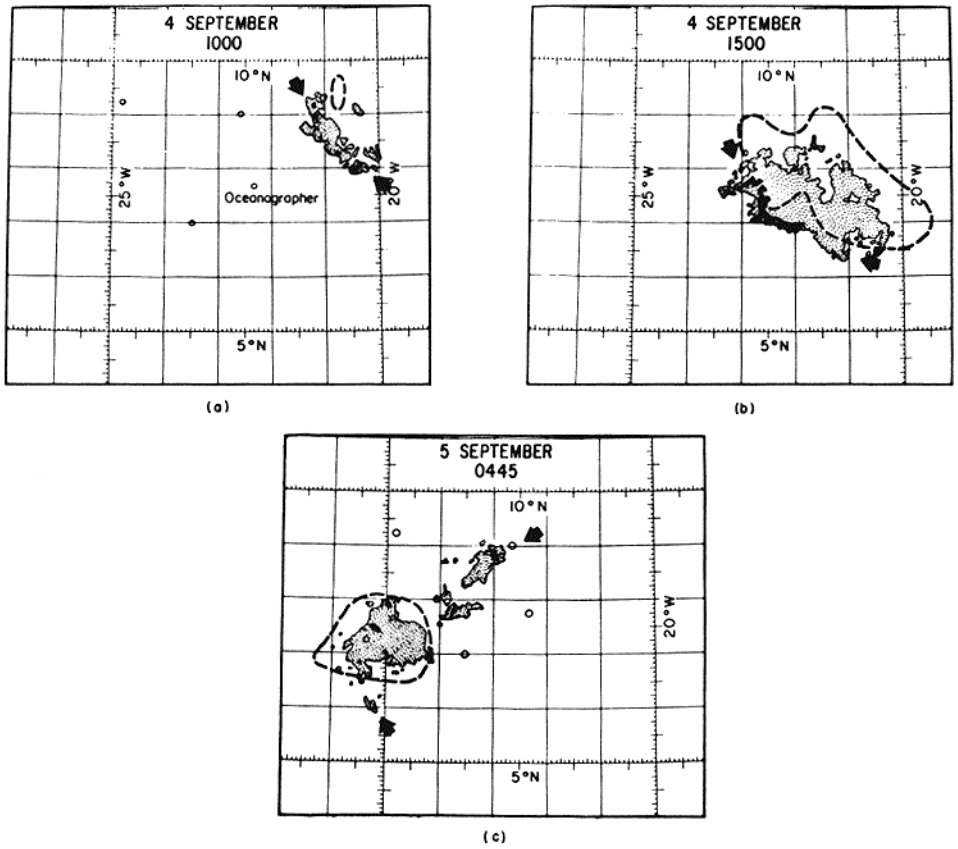

Fig. 19. Life cycle of the cloud and precipitation pattern associated with an equatorial oceanic squall line system. Dotted region encloses low-level precipitation detected by radar. Black indicates regions of precipitation intensity in excess of 38 dBZ or 14 mm h^{-1}. Dashed line is satellite infrared isotherm for −47°C which corresponds to the intersection of the upper level cloud shield with the 11-km level. Arrows locate end points of squall line. Location of Research Vessel *Oceanographer* is indicated in *a*. Data were obtained during the Global Atmospheric Research Programme's Atlantic Tropical Experiment (GATE). Time is in GMT [from *Houze,* 1977].

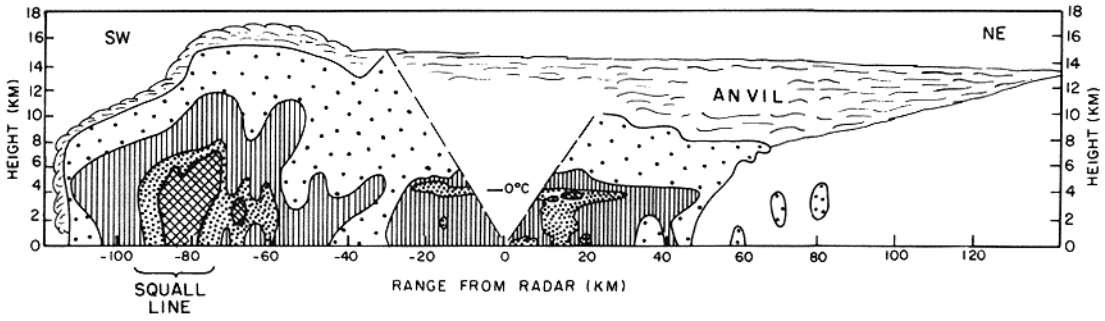

Fig. 20. Vertical cross section through squall line system shown in Figure 19. Horizontal axis runs along azimuths 223° (SW) and 43° (NE) of the *Oceanographer* radar (Figure 19*a*) at 1545 GMT September 4, 1974. Inside contours are for 38, 33, 23 dBZ and minimum detectable echo. Outside scalloped contour outlines cloud boundary estimated from infrared satellited imagery and upper-air sounding data. Storm motion is from NE to SW [from *Houze*, 1977].

of cloud (detected by satellite) penetrating above the 12-km (−47°C) level. By 1500, the squall system was in a mature stage; it had a considerable area covered by high cloud, and region of lighter rain had developed to the rear of the convective line in a manner similar to the mid latitude squall lines considered in section 3.3. By 0445 on September 5, the convective line had almost disappeared, and the remaining precipitation was mainly the light rain falling from the upper level cloud, which itself was shrinking in size. A vertical cross section through the squall-line system in its mature stage (Figure 20) shows the vertically oriented convective cellular structure of the squall line and the highly contrasting stratiform structure of the lighter precipitation falling from the trailing anvil cloud (note the well-defined bright band near the 0°C level). The quantitative significance of the stratiform precipitation is indicated by Figure 21, which shows that the integrated amount of water that fell from the anvil was almost as large as that from the squall line.

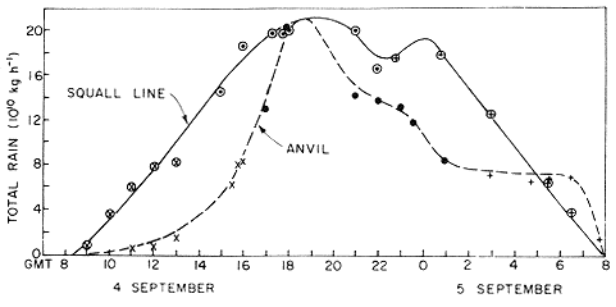

Fig. 21. Total rain integrated over areas covered by squall line and anvil portions of the squall line system. Circled points refer to squall line region [from *Houze*, 1977].

Similar precipitation structure is observed in non-squall cloud clusters. Vertical cross sections through a precipitation area in a non-squall cluster are shown in Figure 22. In its developing stage, the precipitation area was almost entirely convective, with vertical cores of precipitation dominating the radar pattern (Figure 22*a*). As it matured, the precipitation area was convective in its leading portion (near 50 km along B1–B1′ in Figure 22*b*) and more horizontally uniform in its trailing region, particularly along B2–B2′. As the rain area dissipated, it became overwhelmingly stratiform, with the horizontally uniform radar echo extending over a region ≈150 km in width (Figure 22*c*).

4.2 *Monsoon rains*

During the Asian summer, a strong onshore monsoonal flow converges and produces heavy rains over northern India and southeastern Asia. During the Asian winter, there is a strong outpouring of air from east Asia which moves over the South China Sea and converges over Indonesia and Malaysia, where very heavy rainfalls ensue. These summer and winter monsoonal rain areas are the most concentrated regions of condensation in the earth's atmosphere.

As part of the Global Atmospheric Research Programme's Monsoon Experiment (MONEX), the winter monsoon precipitation was studied in detail with a quantitative radar on the northern coast of Borneo, near the center of the winter monsoon

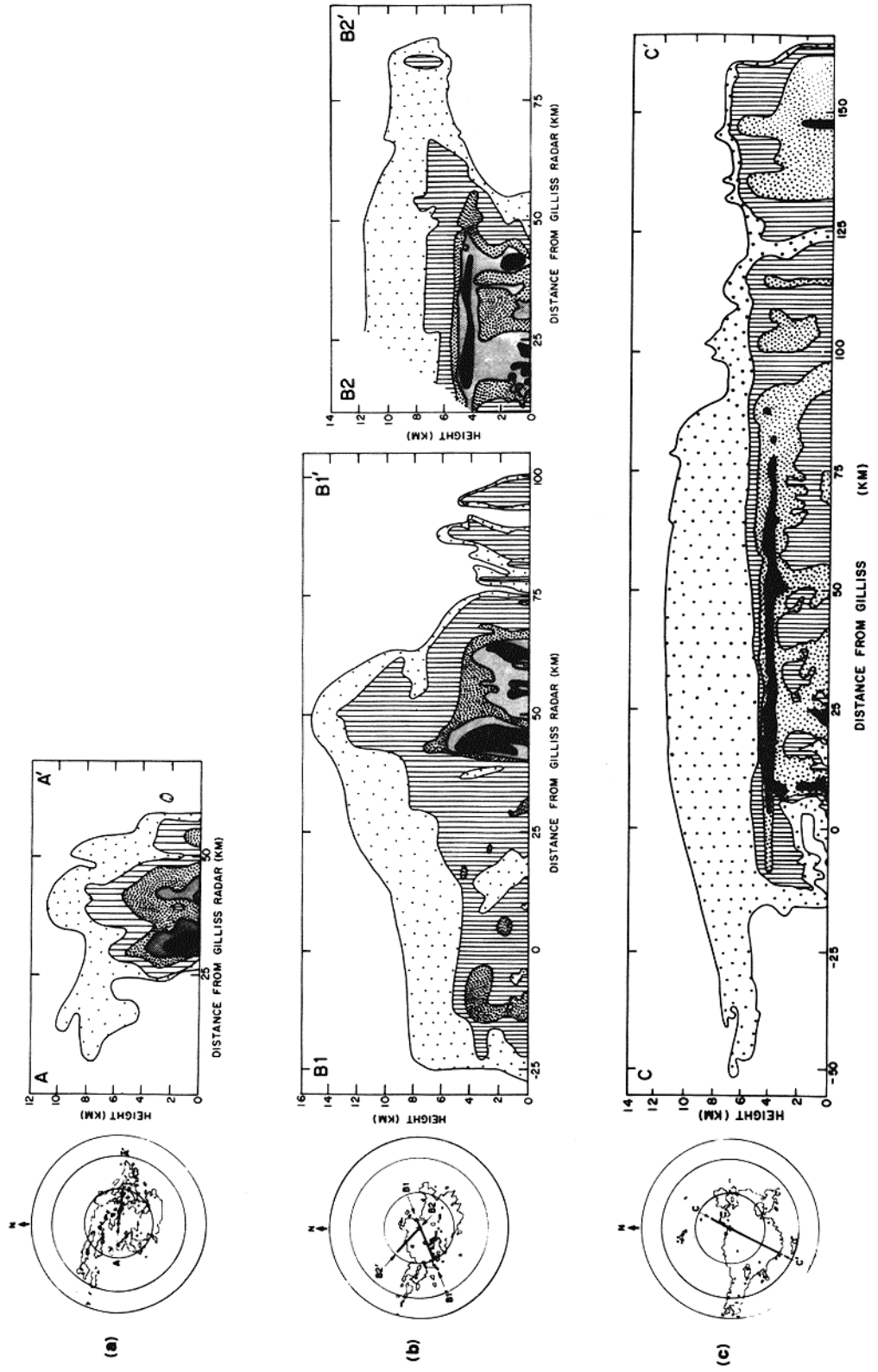

Fig. 22. Mesoscale precipitation feature in a nonsquall tropical cloud cluster. In horizontal cross sections the outside contour of radar reflectivity is for 11 dBZ. The inner contour is for 41 dBZ. Range marks are at 100, 200, and 256 km, and labeled lines identify the vertical cross sections. On the vertical cross sections, the outside contour is for the weakest detectable echo, and the inner contours are for (*a*) 21, 31, 41, and 46 dBZ; (*b*) section B1–B1′: 21, 31, 36, and 41 dBZ; section B2–B2′: 21, 26, 31, and 36 dBZ; (*c*) 26, 31, and 36 dBZ. The data were taken aboard the Research Vessel *Gilliss* (9°N, 25°W) during the Global Atmospheric Research Programme's Atlantic Tropical Experiment (GATE). Times are GMT on September 5, 1974 [from *Leary and Houze*, 1979].

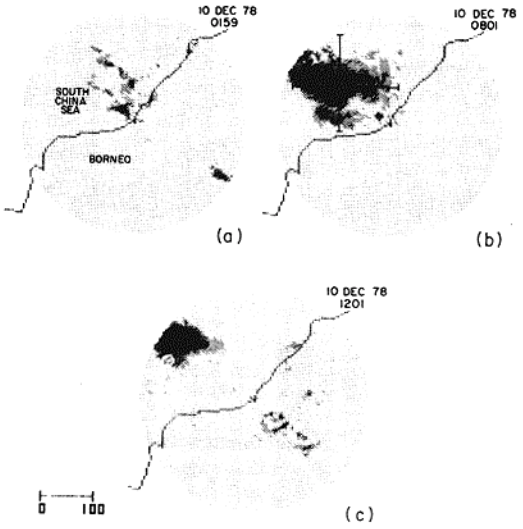

Fig. 23. Low-level radar reflectivity patterns showing the development and dissipation of diurnally generated rain off Borneo on December 10, 1978. Reflectivity is indicated by gray shades with thresholds of 12, 24, and 36 dBZ. Cross hairs in *b* show positions of cross sections in Figure 24 [from *Houze et al.*, 1980].

convergence. The precipitation there underwent a strong, regular diurnal modulation, part of which is illustrated by the example in Figure 23. At 0159 LST, convective cells were forming off the coast of Borneo. By 0801, they had merged into an area of rather uniform rain ≈200 km in horizontal dimension. By 1201, the area had diminished in size and was moving off to the northwest, while daytime convection was forming over land, to the southeast of the radar site. North-south and east-west vertical cross sections through the rain area at 0801 (Figure 24) show that the monsoon precipitation had a structure similar to the cloud clusters described in section 4.1. The precipitation was predominantly stratiform with a well-defined bright band at the melting level (0°C was at about 5 km). Only an occasional convective cell is noted, such as the one near 180 km in the north-south cross section.

4.3 *Hurricanes*

A special type of tropical precipitation system is the hurricane. In these storms, the precipitation is generally arranged in an eyewall rainband, which surrounds the center of the storm, and several outer spiral bands. The rainbands show a mixture of convective and stratiform structure, the latter being evident by the extensive observations of radar bright bands in all quadrants and at most ranges from the storm center [*Black et al.*, 1972; *Hawkins and Imbembo*, 1976]. *Atlas et al.* [1963] obtained a vertical cross section along the axis of an outer spiral rainband (Figure 25) that has a striking similarity in vertical structure to the equatorial cloud cluster and monsoonal precipitation areas described in Sections 4.1 and 4.2. A convectively cellular leading region (between 10 and 35 km) was followed by a horizontally uniform region, some 300 km in dimension, containing a well defined bright band over a distance of ≈100 km.

The hurricane of *Atlas et al.* [1963], though particularly well documented by radar, was observed after it had moved away from its low-latitude region of origin to higher latitudes (off New England). However, the hurricane bright bands noted in the other studies referred to above were observed in storms at low latitudes. Hurricane bright bands cannot, therefore, be regarded as a characteristic

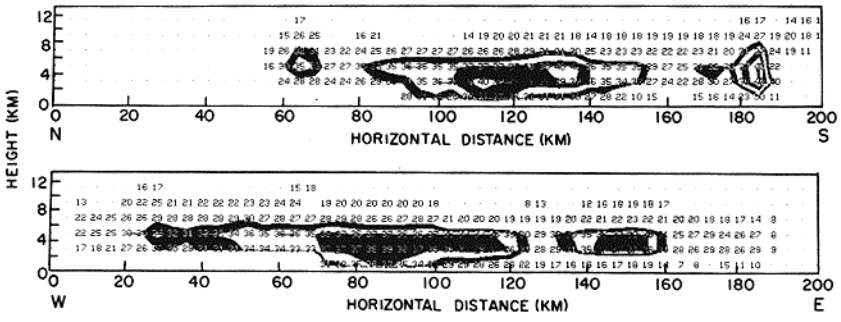

Fig. 24. Vertical cross sections of radar reflectivity through the rain area off Borneo on December 10, 1978. Sections are taken along the (*a*) north-south, and (*b*) west-east cross hairs in Figure 23 [from *Houze et al.*, 1980].

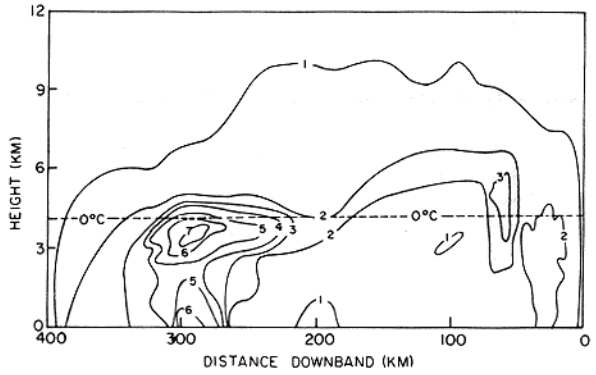

Fig. 25. Vertical cross section of the echo intensity field (in a sequence of gain settings from 1–7) along a hurricane rainband. Echo motion is from left to right [from *Atlas et al.*, 1963].

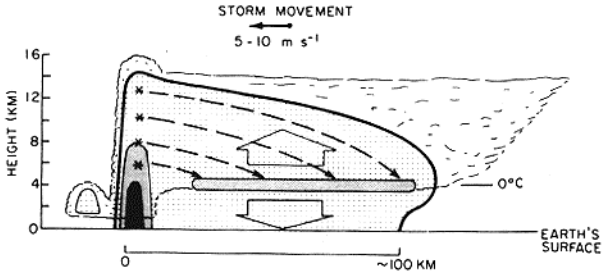

Fig. 26. Schematic of a tropical cloud system. Scalloped boundary surrounds cloud. Solid contours indicate three levels of radar reflectivity, the darkest shading showing the most intense echo. Dashed arrows are ice particle trajectories. Large arrow indicates general lifting above the 4-km level.

that these storms of tropical origin take on as they move to higher latitudes.

5. CONCLUSIONS

Atmospheric precipitation structures can still be thought of as consisting of distinctly stratiform and convective components. However, all the major types of precipitation observed over the globe can be and often are combinations of these two components rather than simply one or the other. Stratiform precipitation develops extensively in tropical precipitation systems as well as in mid-latitudes.

Extratropical cyclonic precipitation is basically stratiform. However, it typically contains convective features, namely, narrow cold frontal rainbands, which can move through the basic stratiform precipitation, and shallow convective cells aloft, which appear to help intensify the stratiform precipitation process in rainbands.

Other precipitation in mid-latitudes and all precipitation in the tropics (except for some orographic precipitation) is basically convective. However, stratiform features can develop in the mid-to-late stages of development of these storms. The extensive stratiform precipitation areas found in the tropics are of this type.

The very considerable horizontal extent of the stratiform precipitation areas of tropical systems (often 100–200 km) is consistent with the conceptual model in Figure 26, in which a storm is assumed to be propagating from right to left at a speed of 5–10 m s^{-1}. The storm is considered to be in a steady state in a coordinate system moving with it, and its propagation is assumed to be occurring by the successive development of new cells at its leading edge. As the mature cells' updrafts cease, ice particles left aloft begin to fall out. In deriving the figure, it was assumed that particles left near the 6-km level fall at 1 m s^{-1}, while those left at 12 km fall at 0.5 m s^{-1}. As the particles move downward, their distance from the storm's leading edge increases as a result of the continued propagation of the leading edge of the system. By the time particles that start falling from the 12-km level reach the 0°C level, they are ~100 km from the mature cells of the storm. This process partially explains the extensive bright band regions that occur in tropical systems and some mid-latitude squall lines.

In tropical squall lines, the postulated process is exaggerated by the wind, which blows through the system horizontally at the rate of a few meters per second everywhere above the melting level. The winds aloft can, therefore, expand the length of the particle trajectories and width of the stratiform region by a factor of two. Interestingly, the widths of the stratiform regions associated with tropical precipitation systems or mid-latitude squall lines are seldom reported to be $\gtrsim$200 km.

Both *Ogura and Liou*'s [1980] observational study of a mid-latitude squall line (cf. Figure 18) and recent numerical modeling of tropical precipitation systems [e.g., *Brown*, 1979] indicate that general lifting, with vertical velocities of the order of tens of centimeters per second, occurs in the anvil clouds from which the stratiform precipitation associated with deep convective phenomena falls. This lifting, represented schematically by the wide arrow in Figure 26, evidently maintains the anvil cloud through which the ice particles left aloft by

the dying convective cells can fall and grow. General subsidence below the base of the anvil cloud shown to be present by *Newton* [1950], *Zipser* [1969], *Ogura and Liou* [1980], and many others, is also shown in the figure.

Thus the wide uniform precipitation areas associated with some convective systems appear to have the basic ingredients of the classical stratiform precipitation mechanism (Figure 1), namely, ice particles formed aloft settling downward through a cloud maintained by weak general lifting. In these cases, the ice particles that are introduced during deep convection remain behind, while the active convective region moves to another location.

For the scientist concerned with radio propagation, as well as for the meteorologist, it perhaps is comforting to see that the traditional concepts of stratiform and convective precipitation still seem to be valid. These two types of structures, however, often occur in complex combinations and the stratiform structures appear to be more prevalent, particularly in the tropics than has previously been recognized.

Acknowledgments. The author has been supported in this work by the Division of Atmospheric Sciences, National Science Foundation (NSF) under grants ATM 77-01344, ATM 78-00232, and ATM 78-16859. The last grant listed is funded jointly by NSF and the GATE Project Office, National Oceanic and Atmospheric Administation (NOAA). Dr. Ralph K. Anderson of NOAA's National Environmental Satellite Service kindly provided the satellite photograph in Figure 4. This paper is contribution 554 of the Department of Atmospheric Sciences, University of Washington.

REFERENCES

Anthes, R. A., H. A. Panofsky, J. J. Cahir, and A. Rango (1978), *The Atmosphere*, 2nd ed., 442 pp., Charles E. Merrill, Columbus, Ohio.

Atlas, D., K. R. Hardy, R. Wexler, and R. J. Boucher (1963), On the origin of hurricane spiral bands, *Geofis. Int.*, *3*(4), 123–132.

Battan, L. J. (1973), *Radar Observations of the Atmosphere*, 324 pp., University of Chicago Press, Chicago, Ill.

Black, P. G., H. V. Senn, and C. L. Courtright (1972), Airborne radar observations of eye configuration changes, bright band distribution, and precipitation tilt during the 1969 multiple seeding experiments in Hurricane Debbie, *Mon. Weather Rev.*, *100*(3), 208–217.

Brown, J. M. (1979), Mesoscale unsaturated downdrafts driven by rainfall evaporation: A numerical study, *J. Atmos. Sci.*, *36*(2), 313–338.

Brown, R. A., L. R. Lemon, and D. A. Burgess (1978), Tornado detection by pulsed Doppler radar, *Mon. Weather Rev.*, *106*(1), 29–38.

Browning, K. A. (1964), Airflow and precipitation trajectories within severe local storms which travel to the right of the winds, *J. Atmos. Sci.*, *21*(6), 634–639.

Browning, K. A. (1974), Mesoscale structure of rain systems in the British Isles, *J. Meteorol. Soc. Jpn.*, *52*(3), 314–327.

Browning, K. A., and D. Atlas (1965), The initial development of a severe storm as observed by radar, *AFCRL-65-695(I), Spec. Rep. 32, NTIS AD-623-787*, pp. 197–236, Air Force Geophysical Lab., Bedford, Mass.

Browning, K. A., and G. B. Foote (1976), Airflow and hail growth in supercell storms and some implications for hail suppresion, *Quart J. R. Meteorol. Soc.*, *102*(433), 499–533.

Browning, K. A., and T. W. Harrold (1970), Air motion and precipitation growth at a cold front, *Quart. J. R. Meteorol. Soc.*, *96*(409), 369–389.

Browning, K. A., J. C. Fankhauser, F. P. Chalon, P. J. Eccles, R. C. Strauch, F. H. Merrem, D. J. Musil, E. L. May, and W. R. Sand (1976), Structure of an evolving hailstorm. Part V: Synthesis and implications for hail growth and hail suppression. *Mon. Weather Rev.*, *104*(5), 603–610.

Byers, H. R., and R. R. Braham, Jr. (1949), *The Thunderstorm*, 287 pp., U. S. Government Printing Office, Washington, D. C.

Chisholm, A. J. (1973), Alberta hailstones, Part I: Radar case studies and airflow models, *Meteorol. Monogr.*, *36*, 1–36.

Dye, J. E., C. A. Knight, V. Toutenhoofd, and T. W. Cannon (1974), The mechanism of precipitation formation in northeastern Colorado cumulus, III. Coordinated microphysical and radar observations and summary, *J. Atmos. Sci.*, *31*(8), 2152–2159.

Foote, G. B. (1977), Response to "The structure and mechanisms of hailstorms," *Meteorol. Monogr.*, *38*, 45–47.

Hamilton, R. A., and J. W. Archbold (1945), Meteorology of Nigeria and adjacent territory, *Quart. J. R. Meteorol. Soc.*, *71*(309–310), 231–264.

Harrold, T. W., and P. M. Austin (1974), The structure of precipitation systems–A review, *J. Rech. Atmos.*, *8*(1–2), 41–57.

Hawkins, H. F., and S. M. Imbembo (1976), The structure of a small, intense hurricane–Inez 1966, *Mon. Weather Rev.*, *104*(4), 418–442.

Hobbs, P. V. (1974), *Ice Physics*, 837 pp., Oxford University Press, New York.

Hobbs, P. V. (1978), Organization and structure of clouds and precipitation on the mesoscale and microscale in cyclonic storms, *Rev. Geophys. Space Phys.*, *16*(4), 741–755.

Hobbs, P. V., and K. R. Biswas (1979), The cellular structure of narrow cold-frontal rainbands, *Quart. J. R. Meteorol. Soc.*, *105*(455), 723–727.

Hobbs, P. V., T. J. Matejka, P. H. Herzegh, J. D. Locatelli, and R. A. Houze, Jr. (1980), The mesoscale and microscale structure and organization of clouds and precipitation in mid-latitude cyclones, I: A case study of a cold front, *J. Atmos. Sci.*, *37*(3), 568–596.

Houghton, H. G. (1968), On precipitation mechanisms and their artificial modification, *J. Appl. Meteorol.* *7*(5), 851–859.

Houze, R. A., Jr. (1977), Structure and dynamics of a tropical squall-line system, *Mon. Weather Rev.*, *105*(12), 1560–1567.

Houze, R. A., and C.-P. Cheng (1977), Radar characteristics of tropical convection observed during GATE: Mean properties and trends over the summer season, *Mon. Weather Rev.*, *105*(8), 964–980.

Houze, R. A., P. V. Hobbs, K. R. Biswas, and W. M. Davis

(1976*a*), Mesoscale rainbands in extratropical cyclones, *Mon. Weather Rev., 104*(7), 868–878.

Houze, R. A., J. D. Locatelli, and P. V. Hobbs (1976*b*), Dynamics and cloud microphysics of the rainbands in an occluded frontal system, *J. Atmos. Sci., 33*(10), 1921–1936.

Houze, R. A., S. G. Geotis, F. D. Marks, Jr., and A. K. West (1980), Observations of winter monsoon clouds and precipitation in the vicinity of north Borneo, in *Communications à la VIIIème Conférence Internationale Sur la Physique des Nuages,* vol. 2, pp. 619–622, La Commission Internationale de Physique de Nuages, L'Association Internationale de Météorologie et Physique de l'Atmosphère, Clermont-Ferrand, France.

Houze, R. A., S. A. Rutledge, T. J. Matejka, and P. V. Hobbs (1981), The mesoscale and microscale structure and organization of clouds and precipitation in mid-latitude cyclones. III: Air motions and precipitation growth in a warm-frontal rainband, *J. Atmos. Sci.,* in press.

James, P. K., and K. A. Browning (1979), Mesoscale structure of line convection at surface cold fronts, *Quart. J. R. Meteorol. Soc., 105*(444), 371–382.

Kessler, E., and R. Wexler (1960), Observations of a cold front, 1 October 1958, *Bull. Am. Meteorol. Soc., 41*(5), 253–257.

Kreitzberg, C. W., and H. A. Brown (1970), Mesoscale weather systems within an occlusion, *J. Appl. Meteorol., 9*(3), 417–432.

Leary, C. A., and R. A. Houze, Jr. (1979), The structure and evolution of convection in a tropical cloud cluster, *J. Atmos. Sci., 36*(3), 437–457.

Lemon, L. R. (1976), The flanking line, a severe thunderstorm intensification source, *J. Atmos. Sci., 33*(4), 686–694.

Lemon, L. R., D. W. Burgess, and R. A. Brown (1978), Tornadic storm airflow and morphology derived from single-Doppler radar measurements, *Mon. Weather Rev., 106*(1), 48–61.

López, R. E. (1976), Radar characteristics of the cloud populations of tropical disturbances in the northwest Atlantic, *Mon. Weather Rev., 104*(3), 268–283.

Ludlam, F. H. (1963), Severe local storms: A review. *Meteorol. Monogr., 27,* 1–30.

Marwitz, J. D. (1972), The structure and motion of severe hailstorms. Part I: Supercell storms, *J. Appl. Meteorol., 11*(1), 166–179.

Matejka, T. J., R. A. Houze, Jr., and P. V. Hobbs (1980), Microphysics and dynamics of clouds associated with mesoscale rainbands in extratropical cyclones, *Quart. J. R. Meteorol. Soc., 106*(447), 29–56.

Newton, C. W. (1950), Structure and mechanism of the prefrontal squall line, *J. Meteorol., 7*(3), 210–222.

Newton, C. W., and J. C. Fankhauser (1975), Movement and propagation of multicellular convective storms, *Pure Appl. Geophys., 113*(5), 747–764.

Ogura, Y., and M.-T. Liou (1980), The structure of a mid-latitude squall line: A case study, *J. Atmos. Sci., 37*(3), 553–567.

Ogura, Y., and T. Takahashi (1971), Numerical simulation of the life cycle of a thunderstorm cell, *Mon. Weather Rev., 99*(12), 895–911.

Payne, S. W., and M. M. McGarry (1977), The relationship of satellite inferred convective activity to easterly waves over West Africa and the adjacent ocean during Phase III of GATE, *Mon. Weather Rev., 105*(4), 413–420.

Sellers, W. D. (1965), *Physical Climatology,* 272 pp., University of Chicago Press, Chicago, Ill.

Zipser, E. J. (1969), The role of organized unsaturated convective downdrafts in the structure and rapid decay of an equatorial disturbance, *J. Appl. Meteorol., 8*(5), 799–814.